water

MDPI

Article

Comparison of Hexavalent Chromium Adsorption Behavior on Conventional and Biodegradable Microplastics

Zongzhi Fang [1], Zhenghua Wang [1,*], Han Tang [1] and Andrew Hursthouse [2]

[1] School of Civil Engineering, Hunan University of Science and Technology, Xiangtan 411201, China; fzz0502by1208@163.com (Z.F.); th02echos@outlook.com (H.T.)
[2] School of Computing, Engineering & Physical Sciences, University of the West of Scotland, Paisley PA1 2BE, UK; andrew.hursthouse@uws.ac.uk
* Correspondence: wzh@hnust.edu.cn

Abstract: Microplastics are omnipresent in aquatic environments and can act as vectors to carry other pollutants, modifying their pathway through the systems. In this study, the differences in the adsorption capacity and mechanism for Cr(VI) sorption with polyethylene (PE, a conventional microplastic) and polylactic acid (PLA, a biodegradable microplastic) were investigated via characterization of the MPs, the determination of kinetic behavior (pseudo-first- and second-order model, the Elovich model), and the degree of fit to Langmuir and Freundlich isothermal models; the adsorption behavior was also studied under different solution conditions. The results indicated that when the dose of MPs was 1 g/L, the adsorption capacity of Cr(VI) on MPs reached the highest value, the adsorption capacities were PLA(0.415 mg/g) > PE(0.345 mg/g). The adsorption of Cr(VI) on PE followed the Langmuir isotherm model, while PLA had a stronger fit with the Freundlich model. Sorption in both cases followed a pseudo-first-order kinetics model. The maximum adsorption capacity of Cr(VI) on PLA (0.54 mg/g) is higher than that on PE (0.38 mg/g). In addition, PLA could reach adsorption equilibrium in about 8 h and can adsorb 72.3% of the total Cr(VI) within 4 h, while PE required 16 h to reach equilibrium, suggesting that PLA adsorbs at a significantly faster rate than PE. Thus, biodegradable MPs like PLA may serve as a superior carrier for Cr(VI) in aquatic environments. When the pH increased from 2 to 6, the adsorption of Cr(VI) by PE and PLA decreased from 0.49 mg/g and 0.52 mg/g to 0.27 mg/g and 0.26 mg/g, respectively. When the concentration of sodium dodecyl sulfate in the Cr(VI) solution was increased from nil to 300 mg/L, the adsorption of Cr(VI) by PE and PLA increased by 3.66 and 3.05 times, respectively. In addition, a higher temperature and the presence of Cu^{2+} and photoaging promoted the adsorption of Cr(VI) by MPs, while higher salinity inhibited the adsorption. The desorption efficiencies of Cr(VI) on MPs were PLA(57.8%) > PE(46.4%). The characterization results further confirmed that the adsorption mechanism could be attributed to electrostatic attraction, hydrogen bonding, and surface complexation. In sum, PLA could potentially serve as better vectors for Cr(VI) than PE, but the risk associated with PLA might be higher than that with PE.

Keywords: microplastics; polylactic acid; polyethylene; Cr(VI); adsorption; desorption; photoaging; surfactant

Citation: Fang, Z.; Wang, Z.; Tang, H.; Hursthouse, A. Comparison of Hexavalent Chromium Adsorption Behavior on Conventional and Biodegradable Microplastics. *Water* **2024**, *16*, 2050. https://doi.org/10.3390/w16142050

Academic Editor: Cidália Botelho

Received: 24 June 2024
Revised: 16 July 2024
Accepted: 17 July 2024
Published: 19 July 2024

1. Introduction

Since the 1950s, plastics have been extensively used across society and in various industries due to their excellent characteristics, such as low cost, flexibility, and durability [1]. However, the stable physical and chemical properties of plastics allow them to persist in the environment for a long time without degradation [2], leading to their accumulation and posing a significant threat to the ecological environment and human health [3]. In 2004, Thompson [4] first reported on an emerging marine pollutant, microplastics (MPs), defined as plastic fragments smaller than 5 mm [5]. Due to their small size, large surface

area, and strong affinity for other pollutants, microplastics pose an even greater risk to the environment [6]. Therefore, the environmental behaviors and ecological effects of microplastics have gained great public interest in recent years [7].

Potentially toxic elements (PTEs) are naturally occurring or anthropogenic elements that have attracted global attention due to their numerous sources, accumulation, persistence, easy enrichment and transfer along the food chain, and resistance to degradation [8–11]. Chromium (Cr), an example of a PTE, is found to be enriched in many types of industrial wastes associated with diverse manufacturing activities [12]. While chromium is an essential trace element for life, Cr(VI) is highly toxic and can be transferred across trophic levels and biomagnification through the food chain, thereby endangering human health and the ecological environment [13]. Studies have shown that microplastics can act as vectors that adsorb PTEs in the environment, migrating and spreading in the form of complexes and endangering ecological safety [14]. It has been reported that PTEs such as Cr, Co, Ni, Cu, Zn, Cd, Hg, Ba, As, and Pb have been detected on the surfaces of microplastics collected on beaches [15,16]. The adsorption process of PTEs on MPs proceeds through the following three discrete steps: (1) diffusion of metals in the thin film around the microplastics; (2) diffusion of metals within the pores of the microplastics; and (3) adsorption on the active surface sites [17].

Due to its wide application, PE, which is commonly used as the primary raw material for everyday plastic products such as films and bags, has become one of the most common plastic pollutants in the environment [18]. PE floating on water surfaces can be easily ingested by aquatic organisms, causing organ damage, cell apoptosis, genetic diseases, or even death [19]. Studies have shown that PE can carry PTEs such as Pb, Cr, Cu, Zn, and Cd [20,21]; the presence of PE increased Cr(VI) accumulation in cucumber (*Cucumis sativus* L.) by 8–39.8%, which reduced chlorophyll content and slowed seedling growth [22]. Similarly, Khan et al. [23] found that the combination of polyvinyl chloride (PVC) and Cr(VI) had severe toxic effects on the physiological and biochemical characteristics of sweet potato, whereas PVC alone did not affect sweet potato, and the accumulation of Cr(VI) increased with increasing doses of PVC. As a common biodegradable plastic, PLA is typically produced from plant-derived starch (like corn, sugarcane, etc.) through fermentation and polymerization processes. Packaging bags made from PLA are degradable, and they can replace traditional plastic bags, which is one of the most effective ways to solve the problem of environmental accumulation of plastic waste [24,25]. However, in natural environments, even biodegradable plastics do not decompose completely in the short term [26] or still require a long time to be fully degraded; thus, they can still form microplastics in the environment, and before complete degradation, they have the characteristics of traditional microplastics [27]. It is equally feasible for PLA to carry PTEs such as Pb, Cu, and Cd, and it may pose potential toxicity to earthworms, invertebrates, etc. [21,24,28,29]. The ecological toxicity of PLA carrying Cd to earthworms is higher than that of conventional microplastics (like PE), severely affecting the normal growth of these organisms [30]. Hence, the environmental impact of biodegradable microplastics is not less than that of traditional microplastics [31]. Many studies on the behavior of traditional microplastics carrying Cr(VI) have been conducted, but the behavior of biodegradable microplastics carrying Cr(VI) is not commonly reported, and developing an understanding of the transport mechanism and factors influencing Cr(VI) by biodegradable compared to traditional microplastics has value. The research on the interaction of MPs with Cr(VI) can help assess their behavior and potential ecological risks in the environment and promote the development of environmental protection and pollution prevention technologies.

This study compared the differences in the adsorption capacity and mechanism of Cr(VI) sorption on the surfaces of PE and PLA. The main goals of this study are to (1) characterize the morphology of microplastics and the changes after adsorption of Cr(VI) using scanning electron microscopy (SEM), Fourier-transform infrared spectroscopy (FTIR), X-ray diffraction (XRD) and X-ray photoelectron spectroscopy (XPS); (2) study the effects of environmental factors (such as pH, salinity, photoaging, surfactants, coexisting ions) on the

adsorption process; and (3) explore the differences in the adsorption mechanism of Cr(VI) between conventional and biodegradable microplastics.

2. Materials and Methods

2.1. Materials

Samples of PE were purchased from Fengtai Plasticizer Co., Ltd. (Dongguan, China), and PLA from Jinheng Plastic Co., Ltd. (Dongguan, China), both with a particle size of 100 mesh, and were not subjected to any further purification. Other chemicals, including $K_2Cr_2O_7$, NaOH, HCl, NaCl, H_3PO_4, HNO_3, H_2SO_4, $CH_3CO\ CH_3$, (Kermel Chemical Reagents Co., Ltd, Tianjin, China) and sodium dodecyl sulfate (SDS) (Maclin Biochemical Technology Co., Ltd, Shanghai, China), were all of analytical-grade purity.

2.2. Batch Adsorption Experiments

To explore the effect of the dose of MPs on the adsorption behavior of Cr on MPs, 25, 50, 100, 150, 200, and 250 mg of MPs powder was weighed into six 100 mL glass bottles separately, and 50 mL of $K_2Cr_2O_7$ solution with a concentration of 10 mg/L was added to make the final reaction volume 50 mL. The pH of the solution was adjusted to 5.0. The glass bottles were placed in a constant temperature (298 K) shaking incubator with 150 r/min. The sampling time was set at 48 h, and an aliquot of 5 mL solution was collected and filtered through a 0.22 μm filter to remove MP particles; the concentration of Cr(VI) was determined by a dual-beam UV-vis spectrophotometer at a wavelength of 540 nm [32].

To investigate the adsorption kinetics, 50 mg of PE and PLA particles were mixed with $K_2Cr_2O_7$ solution with a concentration of 10 mg/L at pH 5.0 and then shaken at a constant temperature of 298 K at 150 rpm. Aliquots (5 mL) were collected at 2, 4, 8, 12, 16, 24, 36, and 48 h [32]; the Cr(VI) concentration detection method is the same as mentioned above.

To examine the adsorption isotherm, 50 mg of PE and PLA particles were mixed with $K_2Cr_2O_7$ solution with 6 concentration gradients (2.5, 5, 7.5, 10, 15, and 20 mg/L) [33] and shaken at 150 rpm at different temperatures (278 K, 288 K, 298 K). The sampling time was set at 24 h to obtain adsorption equilibrium, the collected solution was filtered through a 0.22 μm filter, and then the Cr(VI) concentration was determined using the method mentioned above.

NaOH/HCl (0.1 mol/L) was used to adjust the pH to 2, 3, 4, 5, 6, 7, and 8 to examine the effect of pH [34]. The Cr(VI) solution with NaCl concentrations of 0.05%, 0.1%, 1%, 2%, and 3.5% was prepared to investigate the effect of salinity from 0 to seawater equivalent on the adsorption of Cr(VI) by PE and PLA. To explore the effect of UV aging, 250 mg of MPs and 50 mL of deionized water were placed into a quartz tube, which was then exposed to a 500 W mercury lamp for 48 h. After aging, the MPs were rapidly filtered with deionized water and dried in a 40 °C oven. The adsorption procedure was repeated by mixing the aged MPs and Cr(VI) ions to compare the differences in adsorption between aged and virgin MPs. Various concentrations of SDS (10, 20, 50, 100, and 300 mg/L) and Cu (II) ion (2, 5, 10, 15, and 20 mg/L) were added to the solution, and the adsorption step was repeated to investigate the effect of surfactants and coexisting ions, respectively.

2.3. Desorption Experiments

The desorption experiments were performed after Cr(VI) adsorptions reached equilibrium. The Cr(VI) adsorbed on the PE and PLA were released by changing the nature of the solutions. The following three kinds of solutions were prepared for the desorption experiments: (1) deionized water, pH = 7; (2) 3.5% NaCl solution (simulating seawater); and (3) 50 mg/L SDS solution (simulating surface water with surfactant). A total of 50 mg of Cr(VI)-loaded PE and PLA was weighed into a glass bottle, and 50 mL of the above-mentioned solutions were added to make the final reaction volume 50 mL. Then, the glass bottles were shaken at a constant temperature of 298 K at 150 r/min for 48 h.

2.4. Characterization of MPs

SEM (TESCAN MIRA LMS, Brno, Czech Republic) was used to scan and analyze the surface morphology of the virgin and aged MPs. The sample was prepared by directly adhering the MPs to conductive adhesive, followed by gold sputtering, and analyzed using the secondary electron mode. FTIR (Thermo Scientific Nicolet iS20, Waltham, MA, USA) and XPS (Thermo Scientific ESCALAB Xi, Waltham, MA, USA) were used to analyze the changes in PE and PLA surface groups and elemental chemical states before and after adsorption. The FTIR detection mode was a standard powder compact, with a wavelength range of 400 to 4000 cm^{-1}. XPS characterization included full-spectrum and high-resolution spectra of C1s, O1s, and Cr 2p, with data processing, peak searching and peak fitting. X-ray diffraction (XRD, Rigaku SmartLab SE, Tokyo, Japan) was used to characterize the crystallinity of the MPs before and after adsorption, using a copper target. The scanning angle ranged from 5° to 90°, with a speed of 2°/min.

2.5. Analytical Methods

The amount of Cr(VI) adsorbed by microplastics was calculated using Equation (1), as follows:

$$q_e = \frac{(C_0 - C_e)V}{m} \tag{1}$$

where q_e (mg/g) was the equilibrium adsorption capacity of Cr(VI) on MPs; m (mg) was the mass of microplastics used in the adsorption procedure; V (mL) was the solution volume; C_0 (mg/L) was the initial concentration of Cr(VI) in the solution; and C_e (mg/L) was the equilibrium concentration of Cr(VI) in the solution.

The adsorption efficiency of Cr(VI) by microplastics can be calculated using Equation (2), as follows:

$$adsorption\ efficiency = \frac{(C_0 - C_e)}{C_e} \times 100\% \tag{2}$$

The pseudo-first-order kinetic model, pseudo-second-order kinetic model, and Elovich kinetic model were used to describe the kinetic adsorption of Cr(VI) on microplastics, and the fitting equations were in Equations (3)–(5), respectively.

$$q_t = q_e\left(1 - e^{k_1 t}\right) \tag{3}$$

$$q_t = \frac{k_2 q_e^2 t}{1 + k_2 q_e t} \tag{4}$$

$$q_t = \frac{1}{\beta} ln(\alpha\beta t + 1) \tag{5}$$

where q_t (mg/g) was the adsorption capacity at time t; k_1 (h^{-1})was the reaction rate constant of the pseudo-first-order adsorption kinetics model; k_2 (g/(mg·h)) was the reaction rate constant of the pseudo-second-order adsorption kinetic model; α was the initial adsorption efficiency; and β was the adsorption constants for all experiments.

The Langmuir and Freundlich models were used to describe adsorption isotherms of Cr(VI) on microplastics, and the fitting equations were shown in Equations (6) and (7), respectively, as follows:

$$q_e = \frac{q_m K_l C_e}{1 + K_l C_e} \tag{6}$$

$$q_e = K_f C_e^{1/n} \tag{7}$$

where q_m (mg/g) was the maximum adsorption capacity of Cr(VI) on MPs; K_l (L/mg) was the adsorption affinity constant in the Langmuir model; K_f [(mg/g)·$(L/mg)^{1/n}$] was the adsorption affinity constant in the Freundlich model; and n was a constant in the Freundlich model, representing the supporting force of the adsorption process.

The validity of these models was evaluated by calculating the correlation coefficient (R^2).

The desorption of Cr(VI) from the contaminated MPs can be calculated using Equation (8), as follows:

$$desorption\ efficiency = \frac{C_1}{(c_0 - c_e)} \times 100\% \quad (8)$$

where C_1 (mg/L) was the concentration of Cr(VI) in the solution.

3. Results and Discussion

3.1. Characterization of the Representative Microplastics

3.1.1. Results of SEM

Figure 1 shows the SEM images of virgin PE, aged PE, virgin PLA, and aged PLA. Virgin PE showed an irregular ellipsoidal shape, while PLA showed an irregular blocky structure. The virgin PE surface is smooth, with some microporous porosity (Figure 1a), and the aged PE surface becomes rough with a noticeable wrinkle (Figure 1b). The virgin PLA surface is also smooth, without apparent wrinkles or protrusions (Figure 1c); the aged PLA surface shows flaky protrusions and micropores (Figure 1d). The increase in surface roughness and microporous porosity after aging provides more adsorption sites for MPs to carry PTEs and enhances their adsorption capacity. Additionally, the color of the aged MPs changes from white to pale yellow or yellow, which may be due to the formation of chromophores resulting from oxidation during the aging process [35]. Previous studies have indicated that polyamide (PA) and PVC microplastic surfaces also turn yellow after exposure to ultraviolet light (under laboratory aging conditions) [32,36].

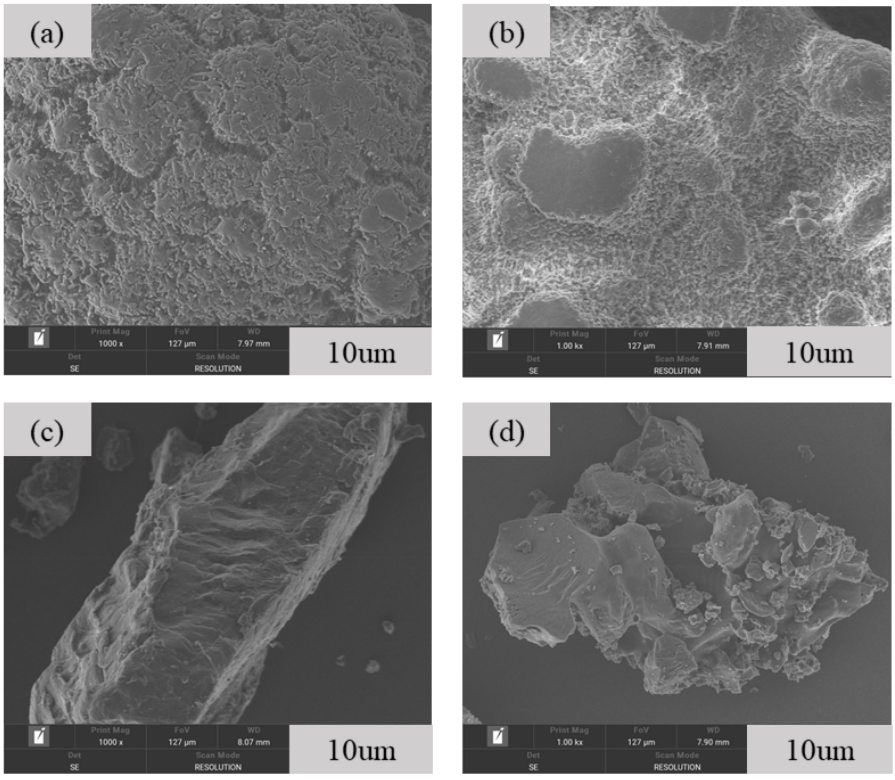

Figure 1. SEM image of virgin PE (**a**), aged PE (**b**), virgin PLA (**c**), and aged PLA (**d**).

3.1.2. Results from XRD and FTIR Analysis

The XRD analysis results are shown in Figure 2a,b. Sharp and amorphous diffraction peaks were found in the XRD patterns of the PE and PLA. The presence of sharp diffraction peaks on the XRD patterns indicated a high degree of crystallinity [37]. Compared to the

freely movable chain structure of PLA, PE requires more energy to break its chain structure, making PLA more likely to interact with pollutants [38]. The characteristic angles for PE are at 21.46°, 23.88°, 30.04°, 36.20°, 39.72°, 42.96°, etc. The characteristic angles for PLA are at 16.42°, 18.68°, 21.22°, etc. The diffraction peaks of PE and PLA carrying Cr(VI) did not show significant shifts, indicating that there was no change in the crystalline composition of the microplastics during the adsorption process [37].

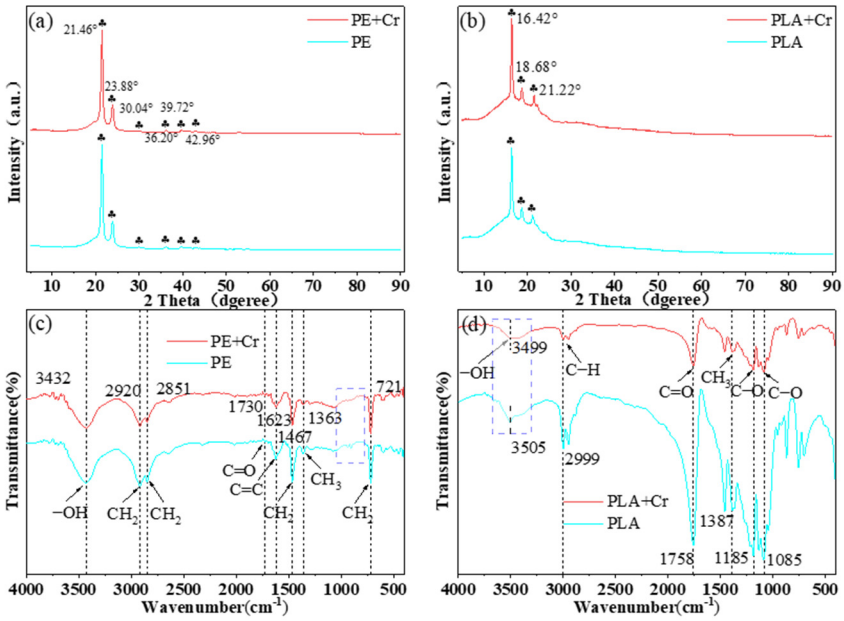

Figure 2. XRD spectra of PE (**a**) and PLA (**b**) before and after Cr (VI) adsorption, and FTIR spectra of PE (**c**) and PLA (**d**) before and after Cr (VI) adsorption.

The FTIR spectra of PE and PLA microplastics before and after adsorption were shown in Figure 2 For PE (Figure 2c); the peaks at 721 cm^{-1}, 1467 cm^{-1}, 2850 cm^{-1}, and 2920 cm^{-1} represented the rocking, bending vibrations, symmetric and asymmetric stretching vibrations of $-CH_2$, respectively. The peaks at 1363 cm^{-1}, 1323 cm^{-1}, and 3432 cm^{-1} were attributed to $-CH_3$, C=C, and −OH, respectively. The peak at 1730 cm^{-1} was associated with the C=O stretching vibration [39,40]. After the adsorption of Cr(VI), the intensity of −OH at 3432 cm^{-1} is weakened, suggesting that −OH may be involved in the adsorption process through hydrogen bonding [38]. The CH_3 vibration at 1363 cm^{-1} shifted to 1358 cm^{-1} after adsorption. Additionally, the C−H bending vibrations at 907 and 938 cm^{-1} were not detected after the adsorption of Cr(VI), indicating that PE likely interacted with Cr(VI). For PLA (Figure 2d), the peaks at 3505 cm^{-1}, 2999 cm^{-1}, 1758 cm^{-1}, and 1387 cm^{-1} corresponded to −OH, C−H, C=O stretching vibration, and C−H bending vibration; the peaks at 1185 cm^{-1} and 1085 cm^{-1} represented C−O vibrations [24]. After the adsorption of Cr(VI), a significant weakening in the intensity of some functional groups, like C=O (1758 cm^{-1}) and C−O (1085 cm^{-1}, 1185 cm^{-1}), was observed, and −OH shifted (from 3505 cm^{-1} to 3499 cm^{-1}), indicating that these functional groups interacted with Cr(VI) [28].

3.1.3. Results of XPS Analysis

The XPS was applied to further demonstrate the changes in the surface functional groups of the microplastics (MPs) before and after the adsorption of Cr(VI) (Figures 3–5). The full spectrum of PE (Figure 3a) showed a relatively simple elemental composition primarily composed of carbon (C), with oxygen (O) also detected, which is likely from additives such as plasticizers introduced during the production process [41]. The C1s spectrum of PE (Figure 4a) indicates that the peak at a binding energy of 284.80 eV corresponds to C−C bonds, and the peak at 285.25 eV represents C−O bonds [32]. After the adsorption of

Cr(VI), the O−C=O in PE's relative atomic percentage decreased from 43.05% to 26.54% (Figure 5a,b). Li et al. [38] also found that the contents of C−O and O−C=O in aged PE after the adsorption of Hg(II) decreased by 3.05% and 7.21%, respectively. For PLA (Figure 3b), the main components detected were the elements C and O. The C1s spectrum of PLA (Figure 4c) is divided into three peaks, corresponding to C−C (284.80 eV), C=O (286.96 eV), and O−C=O (289.03 eV) [38]. After the adsorption of Cr(VI), the binding energy of O−C=O did not change significantly, but its relative atomic percentage decreased by 7.87% (from 47.06% to 39.19%) (Figure 5c,d), indicating that O−C=O groups interacted with Cr(VI) through complexation [38]. This is similar to previous study [42]; after the adsorption of Cu(II), the contents of C−O and O−C=O/C=O in aged PLA decreased by 1.52% and 0.3%, respectively. After the adsorption of Cr(VI) by PE and PLA (Figure 5), the content of −OH groups decreased by 1.08% (from 11.87% to 10.79%) and 3.28% (from 24.57% to 21.29%), respectively. This was consistent with the FTIR findings in which the intensity of −OH in PE weakened after the adsorption of Cr(VI) and the shift and intensity decrease in −OH in PLA, further suggesting that hydrogen bonding might be involved in the adsorption process of Cr(VI) by PE and PLA.

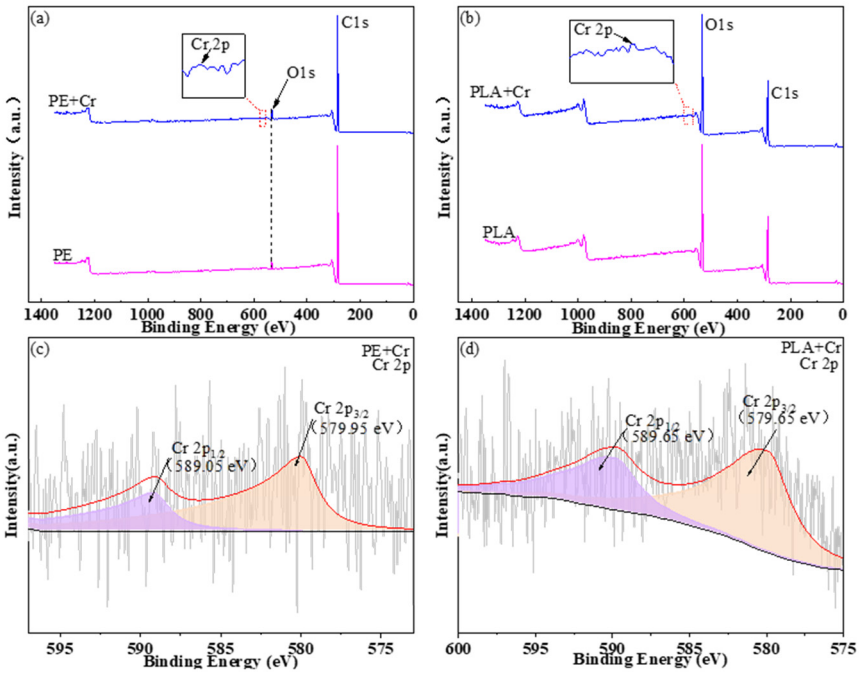

Figure 3. XPS spectra before and after the adsorption of Cr(VI) by PE (**a**) and PLA (**b**) and Cr 2p spectra after the adsorption of Cr(VI) by PE (**c**) and PLA (**d**).

The Cr 2p peaks appeared in PE and PLA after the adsorption of Cr(VI), which were back-convoluted into double peaks, respectively. The binding energies of the Cr 2p peaks were Cr $2p_{1/2}$ (589.05 eV) and Cr $2p_{3/2}$ (579.95 eV) for PE, and the binding energies of the Cr 2p peaks were Cr $2p_{1/2}$ (589.65 eV) and Cr $2p_{3/2}$ (579.65 eV) for PLA, which all corresponded to Cr(VI) [43,44], indicating that Cr(VI) has been successfully adsorbed onto PE and PLA.

3.2. Effect of MP Dose on Adsorption

Figure 6 illustrates the effects of increasing microplastic (MP) doses on the adsorption capacity and efficiency. When the doses of PE and PLA increased from 0.5 g/L to 5 g/L, their adsorption efficiency gradually rose from 1.4% and 1.8% to 5.6% and 7.7%, respectively. Initially, the adsorption capacities of PE and PLA were higher, at doses of 0.5 g/L and 1 g/L. However, as doses increased from 2 g/L to 5 g/L, the adsorption capacities of both PE and PLA decreased slowly. This decrease might be attributed to the increase in total surface area with higher MP doses, which increases the number of adsorbable

sites, consequently leading to a reduction in the adsorption capacity per unit of MP [45]. Taking into account both the adsorption efficiency and capacity, an MP dose of 1 g/L was subsequently selected as the optimal dosage.

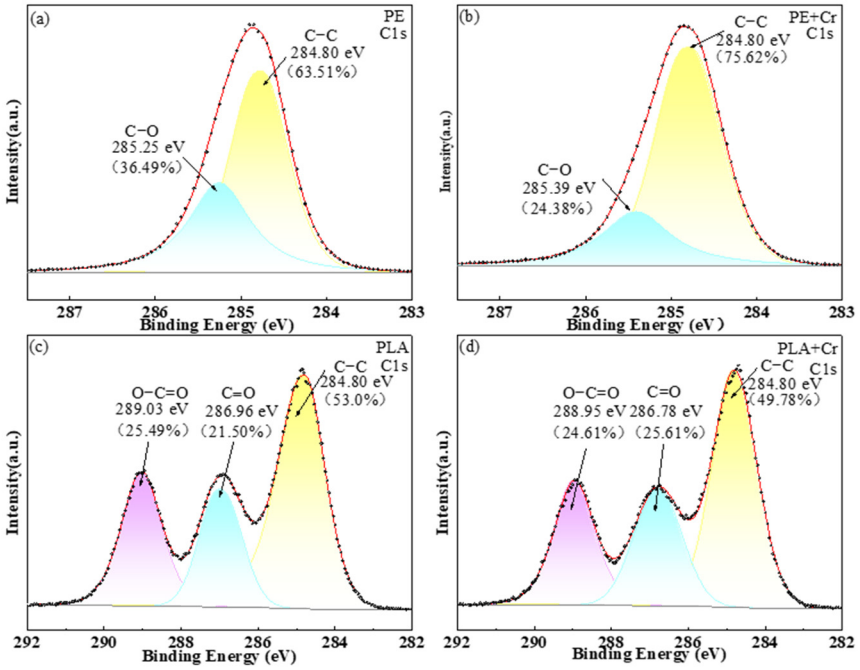

Figure 4. C1s spectra before and after the adsorption of Cr(VI) by PE (**a**,**b**) and PLA (**c**,**d**).

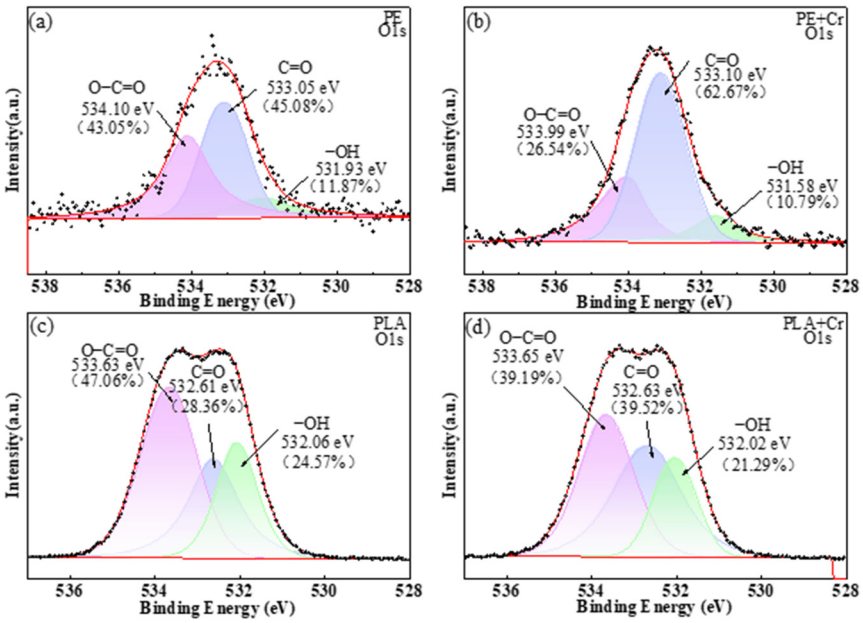

Figure 5. O1s spectra before and after the adsorption of Cr(VI) by PE (**a**,**b**) and PLA (**c**,**d**).

3.3. Adsorption Kinetics of Cr(VI) onto the Representative Microplastics

To investigate the adsorption kinetics of Cr(VI) on PE and PLA microplastics, the pseudo-first-order model, pseudo-second-order model, and Elovich kinetic model were used to fit the adsorption kinetic curves (Figure 7a), and the results were summarized in Table 1. For PE, within 4 h, the adsorption of Cr(VI) on PE increased rapidly, reaching about 52% of the total capacity. From 4 to 16 h, the adsorption capacity increased slowly, and the adsorption equilibrium was reached after 16 h. For PLA, approximately 72.3% of the total Cr(VI) was adsorbed within 4 h. Then, the adsorption procedure slowed within

4 to 8 h, and the adsorption capacity reached up to 90.3% of the total capacity. After 8 h, adsorption equilibrium was reached. The maximum adsorption capacity is greater for PLA (0.415 mg/g) than for PE (0.345 mg/g). The above results indicated that the adsorption process of Cr(VI) on PE and PLA exhibited an initial rapid adsorption stage in which Cr(VI) diffuses from the bulk solution to the outer surface of the MPs through convection, followed by a slower and protracted period in which Cr(VI) penetrates the outer surface of the MPs and diffuses into the micropores. Finally, the adsorption equilibrium stage was reached when Cr(VI) attached to the active sites near the MPs' surface [32].

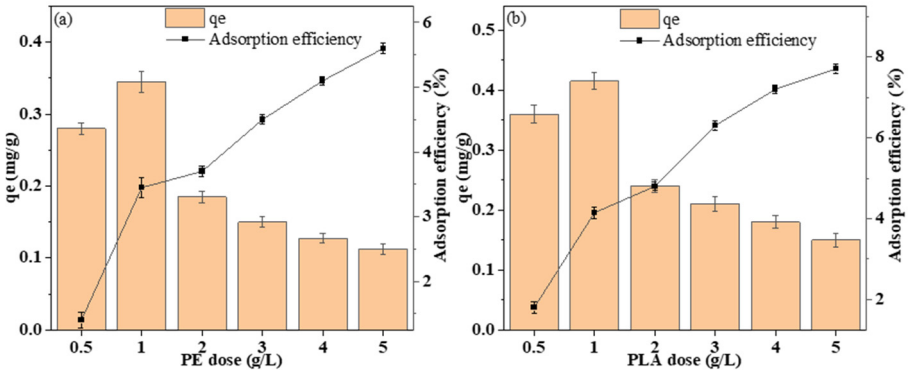

Figure 6. Effect of the dose of PE (**a**) and PLA (**b**) on adsorption.

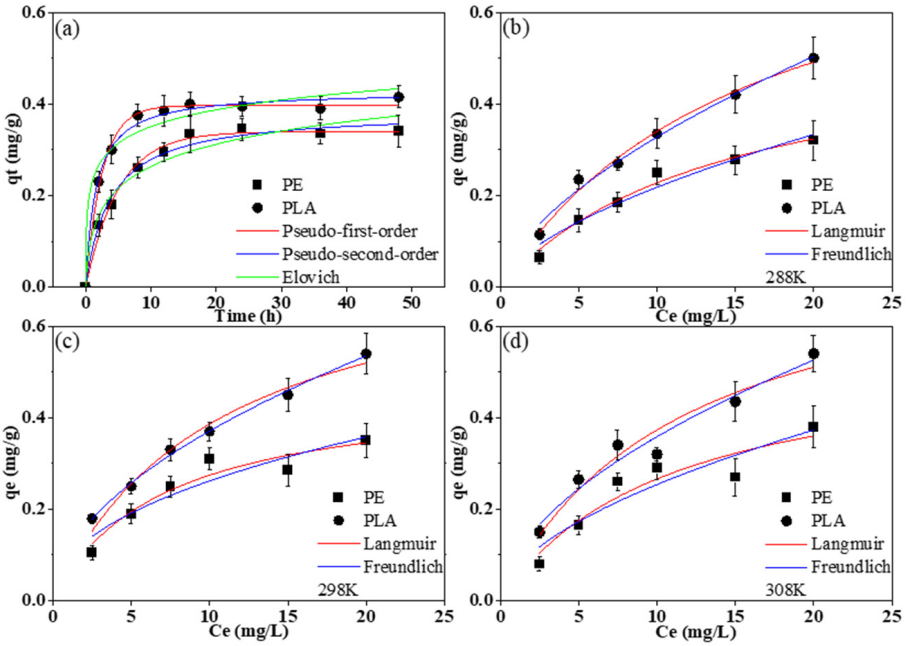

Figure 7. Adsorption kinetics of Cr (VI) on PE and PLA (**a**); isotherms of Cr (VI) by PE and PLA at 288 K (**b**), 298 K (**c**), and 308 K (**d**).

From Table 1, the R^2 for the pseudo-first-order kinetic model for PE and PLA were 0.992 and 0.989, respectively, which were slightly higher than those for the pseudo-second-order kinetic model, which were 0.991 and 0.985. The fitting results of the Elovich model showed that R^2 for both PE and PLA were higher than 0.95, indicating that there are multiple adsorption stages in the adsorption process of Cr(VI) on microplastics [32].

Table 1. Dynamics parameters of Cr (VI) adsorption by PE and PLA.

Model	Parameter	PE	PLA
Pseudo-first-order model	K_1 (h^{-1})	0.198	0.391
	q_e (mg/g)	0.339	0.397
	R^2	0.989	0.993
Pseudo-second-order model	K_2 (g/(mg·h))	0.688	1.464
	q_e (mg/g)	0.384	0.428
	R^2	0.985	0.992
Elovich model	α	0.276	4.001
	β	13.979	18.919
	R^2	0.953	0.961

3.4. Adsorption Isotherms of Cr(VI) Onto the Representative Microplastics

The adsorption isotherm curves of Cr(VI) on PE and PLA were shown in Figure 7b–d, and fitting parameters by Langmuir and Freundlich model were noted in Table 2. According to the R^2 values, the adsorption isotherms of Cr(VI) on PE were better fitted by the Langmuir model (0.875–0.975) than by the Freundlich model (0.839–0.943), indicating that the adsorption process is monolayer adsorption on a homogeneous surface [20]. However, the adsorption isotherms of Cr(VI) on PLA were slightly better fitted by the Freundlich model (0.949–0.985) than by the Langmuir model (0.929–0.988), suggesting that the adsorption of Cr(VI) on PLA may involve multilayer adsorption on a heterogeneous surface, and there might be interactions between adsorbate molecules [16]. Moreover, the $1/n$ values were less than 1, further suggesting that the adsorption is primarily physical [46]. Additionally, the adsorption capacity of PLA for Cr(VI) was 0.54 mg/g, which was significantly higher than that of PE at 0.38 mg/g at 308 K. Previous studies have shown that the maximum adsorption of Cr(VI) on polyamide (PA) and polypropylene (PP) were 2.083 mg/g and 0.114 mg/g, respectively. The high adsorption of Cr(VI) on PA can be explained by the presence of amide groups in PA; these hydrophilic groups favor interactions with Cr(VI) [32].

Comparing the adsorption of Cr(VI) on PE and PLA at different temperatures, it was found that the adsorption capacity gradually increases with the rise in temperature. When the initial concentration of Cr(VI) was 10 mg/L, the adsorption capacity of Cr(VI) on PE changed from 0.25 mg/g at 288 K to 0.31 mg/g at 298 K and 0.29 mg/g at 308 K. The adsorption capacity of Cr(VI) on PLA increased from 0.345 mg/g at 288 K to 0.37 mg/g at 298 K and 0.32 mg/g at 308 K. The adsorption capacity significantly increased when the temperature rose from 288 K to 298 K, while it remained roughly the same or even decreased when the temperature increased from 298 K to 308 K. This could be attributed to the increased random motion caused by higher temperatures promoting adsorption, but at the same time, causing desorption processes among molecules, resulting in a decreased adsorption capacity [41].

3.5. The Influence of Environmental Factors on the Adsorption of Cr(VI) Onto PE and PLA

3.5.1. The Influence of pH and Salinity

As shown in Figure 8a, the adsorption capacity of Cr(VI) on PE and PLA decreased significantly when the pH increased. The highest adsorption capacity of Cr(VI) on PE (0.49 mg/g) and PLA (0.52 mg/g) occurred at pH = 2, and the lowest adsorption capacity of Cr(VI) on PE (0.05 mg/g) and PLA (0.07 mg/g) occurred at pH = 8, which is because Cr(VI) exists in different forms in aqueous solutions at different pH values. At pH = 2–6, Cr(VI) exists in the forms of $HCrO_4^-$ and $Cr_2O_7^{2-}$, and at pH > 6.0, Cr(VI) exists as CrO_4^{2-} [47]. When the pH is less than 3, the surfaces of PE and PLA mainly carry a positive charge [38,48–52], and Cr(VI) in the forms of $HCrO_4^-$ and $Cr_2O_7^{2-}$ is easily adsorbed by the positively charged MPs, hence the high adsorption capacity of Cr(VI) on MPs at this time. As the solution becomes more alkaline, the content of OH^- in the

solution increases and preferentially occupies the adsorption sites on the positively charged MP surface. Moreover, at this point, Cr(VI) exists as CrO_4^{2-}, carrying a higher negative charge, resulting in electrostatic repulsion between MPs and Cr(VI), thereby reducing the adsorption of Cr(VI) on MPs. Additionally, when the pH is higher than 7, Cr(VI) ions in the water begin to form precipitates, which is also one of the reasons for the decreased adsorption capacity of MPs for Cr(VI) in alkaline solutions. These results are similar to those in the study by Zhang et al. [48]; the adsorption capacity of MPs for Cr(VI) decreased from 0.54 mg/g to 0.18 mg/g as the pH was increased from 1.6 to 6.0, indicating that acidic conditions are favorable for the adsorption of Cr(VI) by microplastics and also indicating that electrostatic attraction plays an important role in the adsorption process.

Table 2. Isothermal parameters for the adsorption of Cr (VI) by PE and PLA.

Model	Temperature	Parameter	PE	PLA
Langmuir model	288 K	K_L (L/mg)	0.069	0.063
		q_m (mg/g)	0.559	0.884
		R^2	0.975	0.988
	298 K	K_L (L/mg)	0.144	0.095
		q_m (mg/g)	0.465	0.794
		R^2	0.912	0.975
	308 K	K_L (L/mg)	0.092	0.086
		q_m (mg/g)	0.556	0.806
		R^2	0.875	0.929
Freundlich model	288 K	K_f [(mg/g)·(L/mg)$^{1/n}$]	0.053	0.078
		$1/n$	0.612	0.621
		R^2	0.943	0.985
	298 K	K_f [(mg/g)·(L/mg)$^{1/n}$]	0.093	0.110
		$1/n$	0.451	0.528
		R^2	0.845	0.996
	308 K	K_f [(mg/g)·(L/mg)$^{1/n}$]	0.071	0.100
		$1/n$	0.554	0.553
		R^2	0.839	0.949

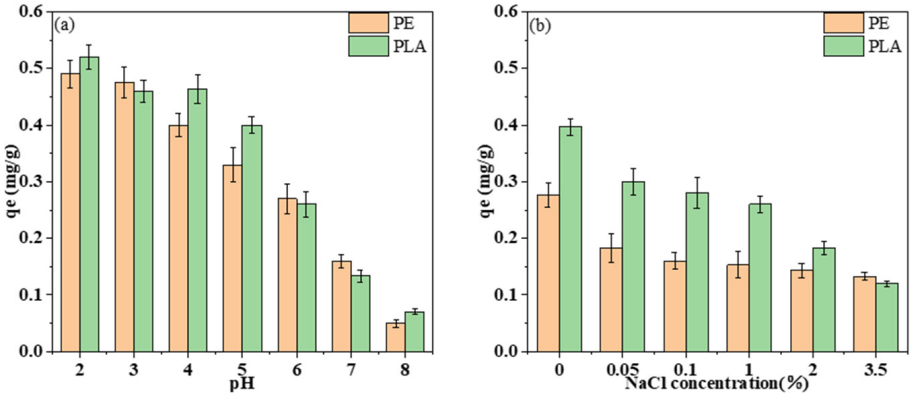

Figure 8. The influence of pH (**a**) and salinity (**b**) on the adsorption of Cr(VI) onto PE and PLA.

As shown in Figure 8b, the effect of NaCl on the adsorption of Cr(VI) on MPs was investigated. The results indicated that the adsorption capacity of MPs for Cr(VI) continually decreased as the concentration of NaCl increased; the adsorption capacity of PE and PLA for Cr(VI) decreased by 0.143 mg/g and 0.277 mg/g, respectively, when the salinity increased from zero to that of seawater. Additionally, it was reported that the maximum

adsorption efficiency of Cr(VI) by PA in deionized water was 66.1%, which was 1.25 times higher than that in simulated seawater. Furthermore, the adsorption capacity of PA for Cr(VI) was negatively correlated with the salt content of the solution. This trend was mainly due to ionic competition and charge screening effects. The ionic competition effect refers to an increase in ionic strength as the concentration of NaCl in water rises, causing Na^+ and Cl^- ions to compete with Cr(VI) for active sites on the surface of the microplastics. Additionally, the increase in these ions might hinder the mass transfer from the aqueous solution to the solid surface, thereby weakening electrostatic interactions [53]. The charge screening effect implies that Na^+ and Cl^- in water might form a charge screening layer on the surface of the microplastics, which would neutralize the surface negative charge of the MPs, thus weakening the electrostatic attraction and hindering the adsorption of Cr(VI) onto the active sites on the surface of the microplastics [54]. Previous studies also found that high concentrations of NaCl in water significantly inhibited the adsorption of Hg(II) and Pb(II) on microplastics. The reason is that Na^+ competes with Hg(II) and Pb(II) for adsorption sites, and a high concentration of Na^+ causes compression of the double layer, reducing the repulsive forces between MPs, leading to aggregation and reducing the surface activity of the microplastics [55,56].

3.5.2. The Influence of Photoaging

The aging process of MPs can be categorized into the following three main types: (1) physical aging, which refers to the mechanical actions such as wear from stones, gravel, or collisions with rocks, waves, and turbulence, leading to smaller fragments of MPs; (2) chemical aging, which is due to chemical actions occurring under the influence of light, heat, or oxidizing agents; and (3) biological aging, which is attributed to the activities of organisms, such as fungi, bacteria, and algae, causing changes in the surface properties of MPs or a reduction in mechanical strength [57].

Aging can lead to an increase in the charge, porosity, roughness, polarity, and hydrophilicity of microplastics, thereby allowing them to adsorb more pollutants [58]. Aging also results in cross-linking, chain scission, and surface yellowing, which is consistent with the phenomena observed in this study. As shown in Figure 9a,b, photoaging promoted the adsorption of Cr(VI) on MPs. At initial concentrations of Cr(VI) of 5, 10, and 20 mg/L, the adsorption capacity of Cr(VI) on aged PE increased by 0.045, 0.020, and 0.050 mg/g compared to the virgin PE, respectively. The adsorption capacity of Cr(VI) on aged PLA increased by 0.035, 0.045, and 0.190 mg/g compared to the virgin PLA. When the initial concentration of Cr(VI) was less than 10 mg/L, the adsorption of Cr(VI) by PE increased with the concentration of Cr(VI); however, when the initial concentration of Cr(VI) was greater than 10 mg/L, the adsorption by PE increased slowly or even slightly decreased. The adsorption of Cr(VI) by PLA increased rapidly with the increase in the initial concentration of Cr(VI), but the increase slowed in the range of 7.5–10 mg/L. The adsorption process of aged PE for Cr(VI) still fitted the Langmuir model well, while PLA was fitted better with the Freundlich model. Liu et al. [20] also found that UV/O_3 aging significantly increased the specific surface area and oxygen content of PE and PLA, enhancing their adsorption capacity for Pb(II). Consequently, the adsorption capacities of Pb(II) on PE and PLA increased from 0.54 mg/g and 0.67 mg/g before aging to 0.83 mg/g and 0.98 mg/g after aging, respectively.

3.5.3. The Influence of the Presence of Surfactants and Cu^{2+}

Surfactants have amphiphilic natures with affinities for both water and oil [50]. Due to the abundant oxygen-containing functional groups in surfactants, they can adhere to the surface of microplastics, affecting the diffusion of microplastics in water, and can bind with PTE ions through complexation or ion exchange. Thus, the presence of surfactants in water can influence the adsorption behavior of PTE ions on microplastics [31]. In this study, SDS was selected as a typical representative to explore the effect of its presence on the adsorption of Cr(VI) by microplastics due to its wide application in cleaning products,

such as shampoos and shower gels. As shown in Figure 10a, the presence of SDS at concentrations of 0–300 mg/L significantly promoted the adsorption of Cr(VI) by PE and PLA. When the concentration of SDS was 300 mg/L, the adsorption capacity of PE and PLA for Cr(VI) increased by 0.83 mg/g and 0.81 mg/g, respectively. This is because increasing the concentration of SDS enhances the dispersion of PE and PLA in aqueous solutions, thereby enhancing the interface interactions between the microplastics and Cr(VI).

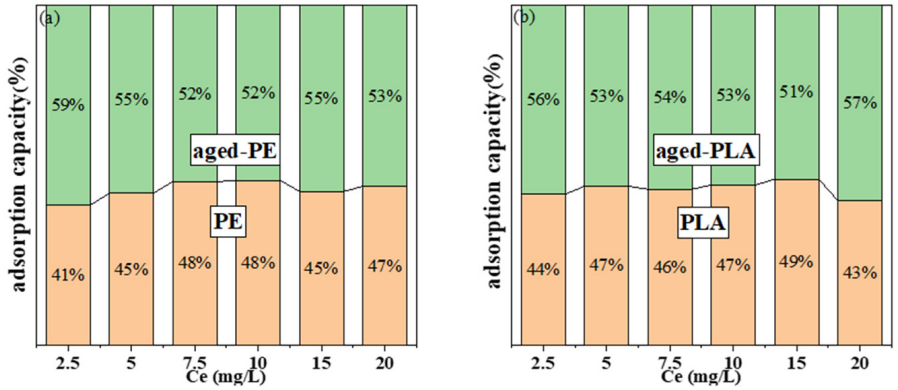

Figure 9. The influence of photoaging on the adsorption of Cr(VI) onto PE (**a**) and PLA (**b**).

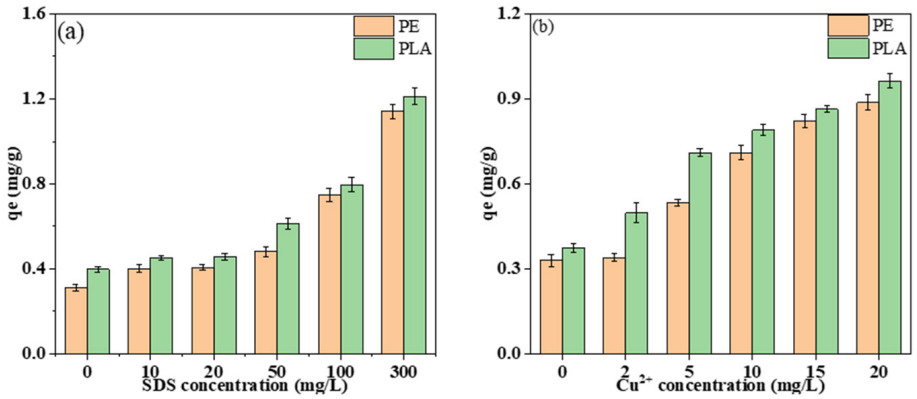

Figure 10. The influence of the presence of surfactants (**a**) and Cu^{2+} (**b**) on the adsorption of Cr(VI) onto PE and PLA.

The critical micelle concentration (CMC) of SDS is approximately 2437 mg/L [50], while the concentration of SDS in this study is far below its CMC value. Below the CMC, a large amount of SDS is in a free state, which promotes the dispersion of MPs in the solution and therefore increases the contact area between MPs and Cr(VI) [48]. Due to the amphiphilic nature of SDS, it can form a thin wetting film on the surface of MPs, creating more adsorbable sites; surfactants can also change the charge on the surface of MPs. SDS molecules may adhere to the rough surface of MPs, increasing the electrostatic interaction between them, thus enhancing the ability of MPs to adsorb PTE ions. Shen et al. [31] found that after adding sodium dodecylbenzene sulfonate (SDBS), the adsorption capacities of Pb(II) on PE, PP, and polymethyl methacrylate (PMMA) increased by 5.19 mg/g, 5.45 mg/g, and 3.66 mg/g, respectively.

As shown in Figure 10b, the presence of Cu^{2+} increased the adsorption capacity of Cr(VI) on PE and PLA, and the adsorption capacity was also increased with the increase in Cu^{2+} concentration. When Cr(VI): Cu^{2+} = 2:1, 1:1, and 1:2, the adsorption capacity of Cr(VI) on PE and PLA increased by 0.20 mg/g, 0.38 mg/g, 0.56 mg/g, 0.34 mg/g, 0.42 mg/g, and 0.59 mg/g, respectively. This indicated that PLA had a stronger affinity for Cr(VI) in solutions containing Cu^{2+}. In conclusion, Cu^{2+} can promote the adsorption of Cr(VI) on PE and PLA, which is mainly due to the following reasons: (1) ion exchange and adsorption bridging effects which can facilitate the adsorption of Cr(VI) by allowing Cu^{2+} to pre-adsorb

onto the MPs and then serve as bridge sites for Cr(VI) adsorption [40]; and (2) the hydration radius of Cr(VI) (0.52 Å) is smaller than that of Cu^{2+} (0.73 Å), making Cr(VI) more readily adsorbed onto active sites [56,59]. Previous research [41] has also suggested that Cu^{2+} could promote the adsorption of Cr(VI) on aged polyethylene and polystyrene because the preferential adsorption of Cu^{2+} could form complexation bonds with the functional groups on the MPs, thereby facilitating further binding of Cr(VI) through a form of cooperative adsorption. Similar results were observed in the study of organic matter adsorption on microplastics, in which the adsorption capacity of ciprofloxacin on 50 μm PE increased from approximately 1.0 mg/g to 2.74 mg/g as the Cu^{2+} concentration increased from 0 to 20 mg/L [40].

3.6. Adsorption Mechanisms

Electrostatic forces, van der Waals forces, hydrogen bonding, and surface complexation are important to the interactions between PTE ions and MPs. From the abovementioned results, the adsorption of Cr(VI) on MPs fitted the pseudo-first-order model well, indicating that the adsorption process was likely a multi-rate process. The effect of pH on the adsorption of Cr(VI) on PE and PLA suggested that the electrostatic repulsion between MPs and metal ions increased with pH increasing, so the electrostatic interaction was the main mechanism for MPs carrying Cr(VI). The structure of PE is stable and not easily broken, while PLA's structure is more mobile and easily disrupted, making it more reactive with other pollutants. Additionally, $-CH_2$ in PE's structure, which cannot adsorb Cr(VI) through ion exchange, may exert adsorption force through valence electron displacement from active electrons on methylene or methyl groups, greatly limiting PE's adsorption performance for PTE ions.

According to the comparison of the FTIR spectra of MPs before and after the adsorption of Cr(VI), there were shifts in some bonds, weakening of functional group intensities, and the disappearance of peaks after PE adsorbed Cr(VI). However, after PLA adsorbed Cr(VI), not only was there a significant weakening of functional group (−OH, C−O, C=O) intensities, but also shifts in functional groups. No significant shifts or new functional groups were found at the characteristic peaks of PE (721 cm^{-1}, 1467 cm^{-1}, 2851 cm^{-1}, 2920 cm^{-1}) and PLA (1185 cm^{-1}, 1387 cm^{-1}, 1758 cm^{-1}, 2999 cm^{-1}). This is in agreement with previous studies; the FTIR spectra of PA and PP after adsorbing Cr(VI) did not differ significantly from those of PA and PP without Cr(VI) adsorption [32]. Similarly, the FTIR spectra of PE and PLA after adsorbing Pb(II) showed no significant changes from those of pristine PE and PLA [59,60]. Therefore, this further suggests that physical adsorption may play a dominant role in the adsorption process.

Combining XPS analysis further elucidates the interaction mechanism. After PE and PLA adsorbed Cr(VI), the binding energies of O−C=O, C=O, and −OH groups changed, and the relative atomic percentages of these oxygen-containing functional groups decreased. Thus, surface complexation and hydrogen bonding also play roles in the adsorption mechanism. Similarly, after the adsorption of rhodamine B on aged polystyrene (PS), the binding energies of O−C=O and C=O changed, and their content decreased by 3.3% [61]. These results highlighted the key role of oxygen-containing functional groups in the adsorption of pollutants by MPs.

Therefore, under low pH conditions, electrostatic attraction is the main mechanism for MPs to accumulate Cr(VI) ions. Surface complexation and hydrogen bonding, primarily involving oxygen-containing functional groups (including C=O, O−C=O, and −OH) with Cr(VI) ions, also contribute to the adsorption process. The schematic structure optimization of PE and PLA and their mechanisms of interaction with Cr(VI) are shown in Figure 11.

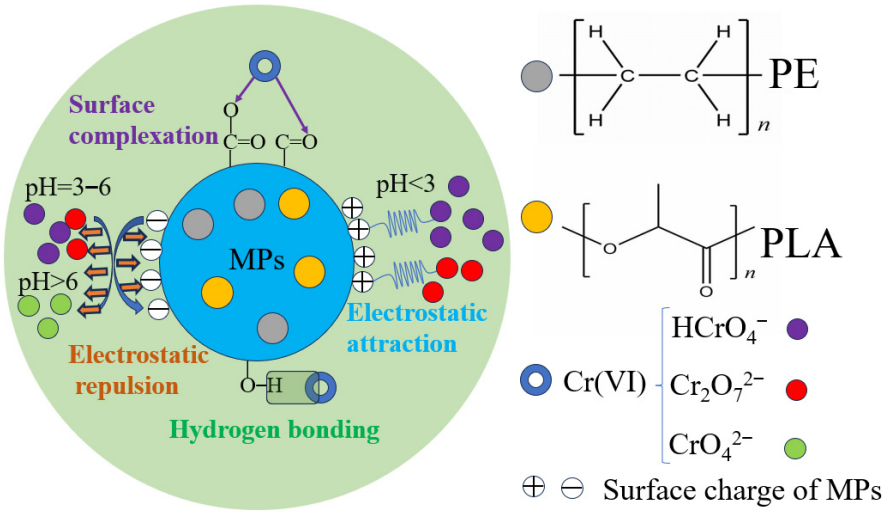

Figure 11. The adsorption mechanisms of Cr(VI) onto PE and PLA.

3.7. Desorption of Cr(VI)

As shown in Figure 12, the desorption capacities of Cr(VI) from the contaminated PE and PLA in three kinds of solutions demonstrated the following order: surfactant solution > simulated seawater > deionized water. Moreover, PLA exhibited higher desorption efficiencies than PE in all three solutions. The desorption efficiencies of Cr(VI) from PLA were 57.8%, 43.4%, and 31.3% in surfactant solution, simulated seawater, and deionized water, respectively, while those from PE were 46.4%, 31.9%, and 23.2%, respectively. The presence of salinity (NaCl) and surfactants promoted desorption, with surfactants having a greater effect than salinity. The promoting effect of salinity is attributed to the disruption of charge balance by salt ions and the competition between Cl^- ions and Cr(VI) [32,38]. Similarly, related studies found that the desorption efficiency of Cr(VI) from PA microplastics was as high as 79.5% in simulated seawater, compared to 34.8% and 66.6% in deionized and simulated freshwater environments, respectively [32]. The desorption of Hg(II) from aged tire particles increased from less than 5 mg/g in ultrapure water to 15.4 mg/g in seawater [38]. With the presence of surfactants, the microplastics floating on the surface of the liquid were dispersed in the solution under the action of the surfactant, increasing their interaction with the solution and thus improving the desorption capacity [39].

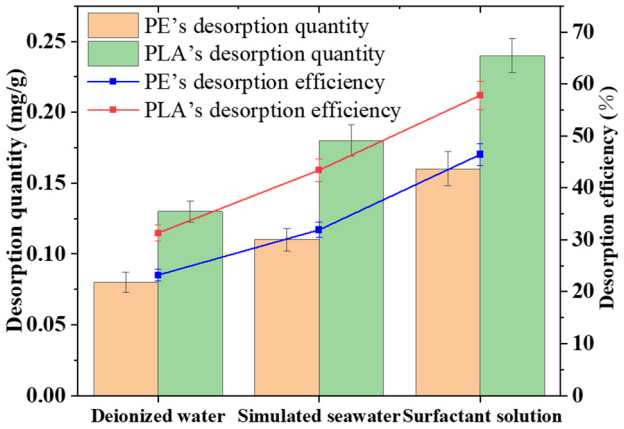

Figure 12. Desorption volume and desorption efficiency of PE and PLA in deionized water, simulated seawater, and surfactant solutions.

4. Conclusions

This study has compared the adsorption behavior of Cr(VI) on conventional (PE) and biodegradable (PLA) microplastics. The adsorption of Cr(VI) on PE was consistent with the Langmuir model, while PLA conformed better to the Freundlich model; both had a close fit with the pseudo-first-order kinetic model, which suggested that both physical and chemical adsorptions occur in the adsorption process, with physical adsorption being dominant. Between the two types of MPs, the adsorption capacity of Cr(VI) on PLA is obviously higher than that of PE. Thus, biodegradable MPs like PLA may be a better carrier for Cr (VI) migration compared to PE in aquatic environments. Higher temperature, the presence of surfactants and Cu^{2+}, and photoaging all promoted the adsorption of Cr(VI) on MPs, while high salinity and pH inhibited adsorption. The highest adsorption capacities of Cr(VI) on PE and PLA were 0.345 mg/g and 0.415 mg/g, respectively, at an MPs dose of 1 g/L. At 308 K, the adsorption capacities of Cr(VI) on PE and PLA were 0.38 mg/g and 0.54 mg/g, respectively. After photoaging, these capacities increased to 0.4 mg/g for PE and 0.73 mg/g for PLA. The optimal pH for adsorption is 2.0, at which the adsorption capacities of Cr(VI) on PE and PLA were 0.49 mg/g and 0.52 mg/g, respectively. With the addition of 20 mg/L Cu^{2+}, the adsorption capacities increase to 0.88 mg/g for PE and 0.96 mg/g for PLA. By adding 300 mg/L SDS, the adsorption capacities of Cr(VI) on PE and PLA reached their maxima of 1.14 mg/g and 1.21 mg/g, respectively. The results of the desorption experiments illustrated that the adsorbed Cr(VI) could be released into the simulated solution in 48 h. Surfactants could improve the desorption of Cr(VI). The desorption efficiencies of Cr(VI) adsorbed on PLA (57.8%) were higher than those on PE(46.4%) in surfactant solution. Results from characterization revealed that both PE and PLA exhibit shifts in functional groups, the weakening of peak intensities, and the disappearance of peaks after the adsorption of Cr(VI). Therefore, the mechanism of MPs adsorbing Cr(VI) may be attributed to electrostatic attraction, hydrogen bonding, and surface complexation. Studying the interactions of microplastics, especially biodegradable microplastics, with PTEs such as chromium helps to understand their migration in the environment, with long-term implications for and effects on ecosystems and human health. Therefore, this study demonstrated PLA's potential as a vector for PTEs, posing a greater threat to the aquatic environment. The risk associated with PLA might be higher than that with PE, and PLA's suitability as a substitute for PE must be thoroughly investigated and confirmed.

Author Contributions: Conceptualization, Z.F. and Z.W.; methodology, Z.F and Z.W.; formal analysis, Z.F.; investigation, Z.F. and H.T.; writing—original draft preparation, Z.F. and H.T.; writing—review and editing, Z.W. and A.H.; supervision, Z.W.; project administration, Z.W.; funding acquisition, Z.W. All authors have read and agreed to the published version of the manuscript.

Funding: This research was funded by the Hunan Provincial Natural Science Foundation of China, grant number 2021JJ30243.

Data Availability Statement: The original contributions presented in this study are included in the article; further inquiries can be directed to the corresponding author.

Conflicts of Interest: The authors declare no conflicts of interest.

References

1. Ghaffar, I.; Rashid, M.; Akmal, M.; Hussain, A. Plastics in the Environment as Potential Threat to Life: An Overview. *Environ. Sci. Pollut. Res.* **2022**, *29*, 56928–56947. [CrossRef] [PubMed]
2. Cózar, A.; Echevarría, F.; González-Gordillo, J.I.; Irigoien, X.; Úbeda, B.; Hernández-León, S.; Palma, Á.T.; Navarro, S.; García-de-Lomas, J.; Ruiz, A.; et al. Plastic Debris in the Open Ocean. *Proc. Natl. Acad. Sci. USA* **2014**, *111*, 10239–10244. [CrossRef] [PubMed]
3. Barros, J.; Seena, S. Plastisphere in Freshwaters: An Emerging Concern. *Environ. Pollut.* **2021**, *290*, 118123. [CrossRef] [PubMed]
4. Thompson, R.C.; Olsen, Y.; Mitchell, R.P.; Davis, A.; Rowland, S.J.; John, A.W.G.; McGonigle, D.; Russell, A.E. Lost at Sea: Where Is All the Plastic? *Science* **2004**, *304*, 838. [CrossRef] [PubMed]

5. He, W.; Chen, X.; Xu, C.; Zhou, C.; Wang, C. Internal Interaction between Chemically-Pretreated Polypropylene Microplastics and Floc Growth during Flocculation: Critical Effect on Floc Properties and Flocculation Mechanisms. *Sep. Purif. Technol.* **2023**, *306*, 122710. [CrossRef]
6. He, W.; Chen, X.; Xu, C.; Zhou, C.; Luo, J. Effect of Microplastic Aging Degree on Filter Cake Formation and Membrane Fouling Characteristics in Ultrafiltration Process with Pre-Coagulation. *Sep. Purif. Technol.* **2023**, *310*, 123221. [CrossRef]
7. He, W.; Zheng, S.; Chen, X.; Lu, D.; Zeng, Z. Alkaline Aging Significantly Affects Mn(II) Adsorption Capacity of Polypropylene Microplastics in Water Environments: Critical Roles of Natural Organic Matter and Colloidal Particles. *J. Hazard. Mater.* **2022**, *438*, 129568. [CrossRef] [PubMed]
8. Dong, L.; Sun, H.; Wang, D.; Wang, S. Enhanced Pb^{2+} Adsorption Using Recyclable Magnetic Sodium Alginate in a Network Structure for High Renewable Capacity. *J. Polym. Eng.* **2024**, *44*, 354–363. [CrossRef]
9. Wang, S.; Liu, Y.; Yang, A.; Zhu, Q.; Sun, H.; Sun, P.; Yao, B.; Zang, Y.; Du, X.; Dong, L. Xanthate-Modified Magnetic Fe_3O_4@SiO_2-Based Polyvinyl Alcohol/Chitosan Composite Material for Efficient Removal of Heavy Metal Ions from Water. *Polymers* **2022**, *14*, 1107. [CrossRef]
10. Dong, L.; Shan, C.; Liu, Y.; Sun, H.; Yao, B.; Gong, G.; Jin, X.; Wang, S. Characterization and Mechanistic Study of Heavy Metal Adsorption by Facile Synthesized Magnetic Xanthate-Modified Chitosan/Polyacrylic Acid Hydrogels. *Int. J. Environ. Res. Public Health* **2022**, *19*, 11123. [CrossRef]
11. Xiong, X.; Wang, J.; Liu, J.; Xiao, T. Microplastics and Potentially Toxic Elements: A Review of Interactions, Fate and Bioavailability in the Environment. *Environ. Pollut.* **2024**, *340*, 122754. [CrossRef] [PubMed]
12. Vaiopoulou, E.; Gikas, P. Regulations for Chromium Emissions to the Aquatic Environment in Europe and Elsewhere. *Chemosphere* **2020**, *254*, 126876. [CrossRef] [PubMed]
13. Monga, A.; Fulke, A.B.; Dasgupta, D. Recent Developments in Essentiality of Trivalent Chromium and Toxicity of Hexavalent Chromium: Implications on Human Health and Remediation Strategies. *J. Hazard. Mater. Adv.* **2022**, *7*, 100113. [CrossRef]
14. Lu, X.; Zeng, F.; Wei, S.; Gao, R.; Abdurahman, A.; Wang, H.; Liang, W. Effects of Humic Acid on Pb^{2+} Adsorption onto Polystyrene Microplastics from Spectroscopic Analysis and Site Energy Distribution Analysis. *Sci. Rep.* **2022**, *12*, 8932. [CrossRef]
15. Acosta-Coley, I.; Mendez-Cuadro, D.; Rodriguez-Cavallo, E.; De La Rosa, J.; Olivero-Verbel, J. Trace Elements in Microplastics in Cartagena: A Hotspot for Plastic Pollution at the Caribbean. *Mar. Pollut. Bull.* **2019**, *139*, 402–411. [CrossRef] [PubMed]
16. Holmes, L.A.; Turner, A.; Thompson, R.C. Adsorption of Trace Metals to Plastic Resin Pellets in the Marine Environment. *Environ. Pollut.* **2012**, *160*, 42–48. [CrossRef]
17. Guo, X.; Wang, J. The Chemical Behaviors of Microplastics in Marine Environment: A Review. *Mar. Pollut. Bull.* **2019**, *142*, 1–14. [CrossRef] [PubMed]
18. Ibarra-Valenzuela, A.P.; Troncoso-Rojas, R.; Islas-Rubio, A.R.; Samsudin, H.; Peralta, E.; Soto-Valdez, H. Replacement of Conventional Packaging with Sustainable Materials for Corn Tortillas. *Food Packag. Shelf Life* **2023**, *40*, 101207. [CrossRef]
19. Yao, Z.; Seong, H.J.; Jang, Y.-S. Environmental Toxicity and Decomposition of Polyethylene. *Ecotoxicol. Environ. Saf.* **2022**, *242*, 113933. [CrossRef]
20. Liu, Y.; Zhang, J.; Cao, W.; Hu, Y.; Shen, W. The Influence of Pb(II) Adsorption on (Non) Biodegradable Microplastics by UV/O_3 Oxidation Treatment. *J. Environ. Chem. Eng.* **2022**, *10*, 108615. [CrossRef]
21. Wang, L.; Guo, C.; Qian, Q.; Lang, D.; Wu, R.; Abliz, S.; Wang, W.; Wang, J. Adsorption Behavior of UV Aged Microplastics on the Heavy Metals Pb(II) and Cu(II) in Aqueous Solutions. *Chemosphere* **2023**, *313*, 137439. [CrossRef] [PubMed]
22. Zhang, Q.; Gong, K.; Shao, X.; Liang, W.; Zhang, W.; Peng, C. Effect of Polyethylene, Polyamide, and Polylactic Acid Microplastics on Cr Accumulation and Toxicity to Cucumber (*Cucumis sativus* L.) in Hydroponics. *J. Hazard. Mater.* **2023**, *450*, 131022. [CrossRef] [PubMed]
23. Khan, M.A.; Kumar, S.; Wang, Q.; Wang, M.; Fahad, S.; Nizamani, M.M.; Chang, K.; Khan, S.; Huang, Q.; Zhu, G. Influence of Polyvinyl Chloride Microplastic on Chromium Uptake and Toxicity in Sweet Potato. *Ecotoxicol. Environ. Saf.* **2023**, *251*, 114526. [CrossRef] [PubMed]
24. Ainali, N.M.; Kalaronis, D.; Evgenidou, E.; Kyzas, G.Z.; Bobori, D.C.; Kaloyianni, M.; Yang, X.; Bikiaris, D.N.; Lambropoulou, D.A. Do Poly(Lactic Acid) Microplastics Instigate a Threat? A Perception for Their Dynamic towards Environmental Pollution and Toxicity. *Sci. Total Environ.* **2022**, *832*, 155014. [CrossRef] [PubMed]
25. Luangrath, A.; Na, J.; Kalimuthu, P.; Song, J.; Kim, C.; Jung, J. Ecotoxicity of Polylactic Acid Microplastic Fragments to Daphnia Magna and the Effect of Ultraviolet Weathering. *Ecotoxicol. Environ. Saf.* **2024**, *271*, 115974. [CrossRef]
26. Chamas, A.; Moon, H.; Zheng, J.; Qiu, Y.; Tabassum, T.; Jang, J.H.; Abu-Omar, M.; Scott, S.L.; Suh, S. Degradation Rates of Plastics in the Environment. *ACS Sustain. Chem. Eng.* **2020**, *8*, 3494–3511. [CrossRef]
27. Zhang, L.; Luo, Y.; Zhang, Z.; Pan, Y.; Li, X.; Zhuang, Z.; Li, J.; Luo, Q.; Chen, X. Enhanced Reproductive Toxicity of Photodegraded Polylactic Acid Microplastics in Zebrafish. *Sci. Total Environ.* **2024**, *912*, 168742. [CrossRef]
28. Sun, Y.; Wang, X.; Xia, S.; Zhao, J. Cu(II) Adsorption on Poly(Lactic Acid) Microplastics: Significance of Microbial Colonization and Degradation. *Chem. Eng. J.* **2022**, *429*, 132306. [CrossRef]
29. Tian, X.; Weixie, L.; Wang, S.; Zhang, Y.; Xiang, Q.; Yu, X.; Zhao, K.; Zhang, L.; Penttinen, P.; Gu, Y. Effect of Polylactic Acid Microplastics and Lead on the Growth and Physiological Characteristics of Buckwheat. *Chemosphere* **2023**, *337*, 139356. [CrossRef] [PubMed]

30. Shang, G.; Zhai, J.; Xu, G.; Wang, L.; Wang, X. Ecotoxicological Effects of Co-Exposure Biodegradable Microplastics Polylactic Acid with Cadmium Are Higher than Conventional Microplastics Polystyrene with Cadmium on the Earthworm. *Sci. Total Environ.* **2023**, *903*, 166953. [CrossRef]
31. Shen, M.; Song, B.; Zeng, G.; Zhang, Y.; Teng, F.; Zhou, C. Surfactant Changes Lead Adsorption Behaviors and Mechanisms on Microplastics. *Chem. Eng. J.* **2021**, *405*, 126989. [CrossRef]
32. Shao, X.; Zhang, Q.; Liang, W.; Gong, K.; Fu, M.; Saif, S.; Peng, C.; Zhang, W. Polyamide Microplastics as Better Environmental Vectors of Cr(VI) in Comparison to Polyethylene and Polypropylene Microplastics. *Mar. Pollut. Bull.* **2023**, *186*, 114492. [CrossRef] [PubMed]
33. Mohanty, S.; Benya, A.; Hota, S.; Kumar, M.S.; Singh, S. Eco-Toxicity of Hexavalent Chromium and Its Adverse Impact on Environment and Human Health in Sukinda Valley of India: A Review on Pollution and Prevention Strategies. *Environ. Chem. Ecotoxicol.* **2023**, *5*, 46–54. [CrossRef]
34. Assefa, H.; Singh, S.; Olu, F.E.; Dhanjal, D.S.; Mani, D.; Khan, N.A.; Singh, J.; Ramamurthy, P.C. Advances in Adsorption Technologies for Hexavalent Chromium Removal: Mechanisms, Materials, and Optimization Strategies. *Desalination Water Treat.* **2024**, *319*, 100576. [CrossRef]
35. Lv, Y.; Huang, Y.; Kong, M.; Yang, Q.; Li, G. Multivariate Correlation Analysis of Outdoor Weathering Behavior of Polypropylene under Diverse Climate Scenarios. *Polym. Test.* **2017**, *64*, 65–76. [CrossRef]
36. Fan, X.; Zou, Y.; Geng, N.; Liu, J.; Hou, J.; Li, D.; Yang, C.; Li, Y. Investigation on the Adsorption and Desorption Behaviors of Antibiotics by Degradable MPs with or without UV Ageing Process. *J. Hazard. Mater.* **2021**, *401*, 123363. [CrossRef]
37. Zhang, M.; Liu, N.; Hou, L.; Li, C.; Li, C. Adsorption Behaviors of Chlorpyrifos on UV Aged Microplastics. *Mar. Pollut. Bull.* **2023**, *190*, 114852. [CrossRef] [PubMed]
38. Li, L.; Xue, B.; Lin, H.; Lan, W.; Wang, X.; Wei, J.; Li, M.; Li, M.; Duan, Y.; Lv, J.; et al. The Adsorption and Release Mechanism of Different Aged Microplastics toward Hg(II) via Batch Experiment and the Deep Learning Method. *Chemosphere* **2024**, *350*, 141067. [CrossRef]
39. Jiang, Y.; Qin, Z.; Fei, J.; Ding, D.; Sun, H.; Wang, J.; Yin, X. Surfactant-Induced Adsorption of Pb(II) on the Cracked Structure of Microplastics. *J. Colloid Interface Sci.* **2022**, *621*, 91–100. [CrossRef]
40. Lv, M.; Zhang, T.; Ya, H.; Xing, Y.; Wang, X.; Jiang, B. Effects of Heavy Metals on the Adsorption of Ciprofloxacin on Polyethylene Microplastics: Mechanism and Toxicity Evaluation. *Chemosphere* **2023**, *315*, 137745. [CrossRef]
41. Li, Y.; Zhang, Y.; Su, F.; Wang, Y.; Peng, L.; Liu, D. Adsorption Behaviour of Microplastics on the Heavy Metal Cr(VI) before and after Ageing. *Chemosphere* **2022**, *302*, 134865. [CrossRef] [PubMed]
42. Huang, W.; Zhang, J.; Zhang, Z.; Gao, H.; Xu, W.; Xia, X. Insights into Adsorption Behavior and Mechanism of Cu(II) onto Biodegradable and Conventional Microplastics: Effect of Aging Process and Environmental Factors. *Environ. Pollut.* **2024**, *342*, 123061. [CrossRef] [PubMed]
43. Cai, Y.; Ran, Z.; Cang, Y.; Chen, X.; Shaaban, M.; Peng, Q.-A. Efficient Removal of Cr(VI) and As(V) from an Aquatic System Using Iron Oxide Supported Typha Biochar. *Environ. Res.* **2023**, *225*, 115588. [CrossRef] [PubMed]
44. Qin, X.; Tao, R.; Cheng, S.; Xing, B.; Meng, W.; Nie, Y.; Zhang, C.; Yu, J. Microwave-Assisted One-Pot Method Preparation of ZnO Decorated Biochar for Levofloxacin and Cr(VI) Removal from Wastewater. *Ind. Crops Prod.* **2024**, *208*, 117863. [CrossRef]
45. Li, H.; Wang, F.; Li, J.; Deng, S.; Zhang, S. Adsorption of Three Pesticides on Polyethylene Microplastics in Aqueous Solutions: Kinetics, Isotherms, Thermodynamics, and Molecular Dynamics Simulation. *Chemosphere* **2021**, *264*, 128556. [CrossRef] [PubMed]
46. Wang, X.; Zhang, R.; Li, Z.; Yan, B. Adsorption Properties and Influencing Factors of Cu(II) on Polystyrene and Polyethylene Terephthalate Microplastics in Seawater. *Sci. Total Environ.* **2022**, *812*, 152573. [CrossRef] [PubMed]
47. Zhao, Y.; Zhang, X.; Liu, W.; Li, M.; Chen, Y.; Yang, Y.; Yang, S. Simple Synthesis, Characterization and Mechanism of Fe/Zr Bimetallic-Organic Framework for Cr (VI) Removal from Wastewater. *J. Environ. Chem. Eng.* **2024**, *12*, 112040. [CrossRef]
48. Zhang, W.; Zhang, L.; Hua, T.; Li, Y.; Zhou, X.; Wang, W.; You, Z.; Wang, H.; Li, M. The Mechanism for Adsorption of Cr(VI) Ions by PE Microplastics in Ternary System of Natural Water Environment. *Environ. Pollut.* **2020**, *257*, 113440. [CrossRef]
49. Plohl, O.; Erjavec, A.; Fras Zemljič, L.; Vesel, A.; Čolnik, M.; Škerget, M.; Fan, Y.V.; Čuček, L.; Trimmel, G.; Volmajer Valh, J. Morphological, Surface and Thermal Properties of Polylactic Acid Foils, Melamine-Etherified Resin, and Polyethylene Terephthalate Fabric during (Bio)Degradation in Soil. *J. Clean. Prod.* **2023**, *421*, 138554. [CrossRef]
50. Huang, W.; Deng, J.; Liang, J.; Xia, X. Comparison of Lead Adsorption on the Aged Conventional Microplastics, Biodegradable Microplastics and Environmentally-Relevant Tire Wear Particles. *Chem. Eng. J.* **2023**, *460*, 141838. [CrossRef]
51. Wang, Y.; Wang, X.; Li, Y.; Li, J.; Liu, Y.; Xia, S.; Zhao, J. Effects of Exposure of Polyethylene Microplastics to Air, Water and Soil on Their Adsorption Behaviors for Copper and Tetracycline. *Chem. Eng. J.* **2021**, *404*, 126412. [CrossRef]
52. Lin, Z. Comparative Analysis of Kinetics and Mechanisms for Pb(II) Sorption onto Three Kinds of Microplastics. *Ecotoxicol. Environ. Saf.* **2021**, *208*, 111451. [CrossRef]
53. You, H.; Cao, C.; Sun, X.; Huang, B.; Qian, Q.; Chen, Q. Microplastics as an Emerging Vector of Cr(VI) in Water: Correlation of Aging Properties and Adsorption Behavior. *Sci. Total Environ.* **2023**, *904*, 166480. [CrossRef] [PubMed]
54. Yu, A.; Sun, X.; Tang, S.; Zhang, Y.; Li, M.; Wang, X. Adsorption Mechanism of Cadmium on Polystyrene Microplastics Containing Hexabromocyclododecane. *Environ. Technol. Innov.* **2021**, *24*, 102036. [CrossRef]
55. Gao, Z.; Cizdziel, J.V.; Wontor, K.; Olubusoye, B.S. Adsorption/Desorption of Mercury (II) by Artificially Weathered Microplastics: Kinetics, Isotherms, and Influencing Factors. *Environ. Pollut.* **2023**, *337*, 122621. [CrossRef]

56. He, W.; Wang, X.; Zhang, Y.; Zhu, B.; Wu, H. Adsorption Behavior of Aged Polystyrene Microplastics (PSMPs) for Manganese in Water: Critical Role of Hydrated Functional Zone Surrounding the Microplastic Surface. *J. Environ. Chem. Eng.* **2022**, *10*, 109040. [CrossRef]
57. Yu, X.; Wang, B.; Han, C.; Liu, L.; Han, X.; Zheng, B.; Zhang, B.; Sun, J.; Zhang, Z.; Ma, W.; et al. Physicochemical and Biological Changes on Naturally Aged Microplastic Surfaces in Real Environments over 10 Months. *Environ. Pollut.* **2023**, *337*, 122522. [CrossRef]
58. Brandon, J.; Goldstein, M.; Ohman, M.D. Long-Term Aging and Degradation of Microplastic Particles: Comparing In Situ Oceanic and Experimental Weathering Patterns. *Mar. Pollut. Bull.* **2016**, *110*, 299–308. [CrossRef] [PubMed]
59. Liu, S.; Huang, J.; Zhang, W.; Shi, L.; Yi, K.; Zhang, C.; Pang, H.; Li, J.; Li, S. Investigation of the Adsorption Behavior of Pb(II) onto Natural-Aged Microplastics as Affected by Salt Ions. *J. Hazard. Mater.* **2022**, *431*, 128643. [CrossRef]
60. Yu, Y.; Ding, Y.; Zhou, C.; Ge, S. Aging of Polylactic Acid Microplastics during Hydrothermal Treatment of Sewage Sludge and Its Effects on Heavy Metals Adsorption. *Environ. Res.* **2023**, *216*, 114532. [CrossRef]
61. Wang, K.; Kou, Y.; Guo, C.; Wang, K.; Li, J.; Schmidt, J.; Wang, M.; Liang, S.; Wang, W.; Lu, Y.; et al. Comparison of Rhodamine B Adsorption and Desorption on the Aged Non-Degradable and Degradable Microplastics: Effects of Charge-Assisted Hydrogen Bond and Underline Mechanism. *Environ. Technol. Innov.* **2024**, *35*, 103739. [CrossRef]